

## ARTICLE

Received 6 Aug 2013 | Accepted 10 Feb 2014 | Published 4 Mar 2014

DOI: 10.1038/ncomms4417

# Frictional velocity-weakening in landslides on Earth and on other planetary bodies

Antoine Lucas<sup>1,2,†</sup>, Anne Mangeney<sup>1,3</sup> & Jean Paul Ampuero<sup>2</sup>

One of the ultimate goals in landslide hazard assessment is to predict maximum landslide extension and velocity. Despite much work, the physical processes governing energy dissipation during these natural granular flows remain uncertain. Field observations show that large landslides travel over unexpectedly long distances, suggesting low dissipation. Numerical simulations of landslides require a small friction coefficient to reproduce the extension of their deposits. Here, based on analytical and numerical solutions for granular flows constrained by remote-sensing observations, we develop a consistent method to estimate the effective friction coefficient of landslides. This method uses a constant basal friction coefficient that reproduces the first-order landslide properties. We show that friction decreases with increasing volume or, more fundamentally, with increasing sliding velocity. Inspired by frictional weakening mechanisms thought to operate during earthquakes, we propose an empirical velocity-weakening friction law under a unifying phenomenological framework applicable to small and large landslides observed on Earth and beyond.

<sup>1</sup>Équipe de sismologie, Institut de Physique du Globe de Paris, Sorbone Paris Cité, Université Paris Diderot, UMR 7154 CNRS, 1 rue Jussieu, 75238 Paris cedex 05, France. <sup>2</sup>Division of Geological and Planetary Sciences, California Institute of Technology, 1200 E. California Blvd, Pasadena, California 95125, USA. <sup>3</sup>Équipe ANGE INRIA, Laboratoire Jacques-Louis Lions, UPMC Paris 6, 4 place Jussieu, Case 187 75252 Paris cedex 05, France. † Present address: Laboratoire Astrophysique, Instrumentation et Modélisation (AIM), CNRS-UMR 7158, Université Paris-Diderot, CEA-Saclay, Gif-sur-Yvette 91191, France. Correspondence and requests for materials should be addressed to A.L. (email: lucas@ipgp.fr).

**A**valanches, debris flows and landslides are key components of mass transport at the surface of the Earth. They have also been observed on other planetary bodies of our Solar System, from the interior planets to the icy moons of Saturn as well as small bodies such as the asteroid Vesta<sup>1</sup>. On Earth these mass wasting processes feed rivers with solid materials and thus participate in the evolution of the landscape. Moreover, catastrophic landslides constitute a significant hazard for life and property. The great diversity of natural gravitational flows in terms of volumes involved (from a few cubic metres to hundreds of cubic kilometres), flowing materials (for example, soil, clay, rocks, water ice and mixtures of different materials with or without the presence of a fluid phase such as gas or water), environment (for example, different gravitational acceleration on different planetary bodies, underlying topography), triggering mechanisms (seismic, volcanic, hydrological and climatic external forcing) and physical processes involved during the flow (for example, fragmentation<sup>2</sup> and erosion/deposition<sup>3,4</sup>) hinder a unified view of these phenomena. Therefore, despite the great number of experimental, theoretical and field studies, the behaviour of natural landslides is still poorly understood. This prevents accurate estimation of their maximum travel distance (also known as runout distance), the area covered by the flows and of their velocity, which are crucial components of hazard assessment for these catastrophic events. Calculating these quantities requires the use of appropriate laws describing energy dissipation during the landslide. Much research has been carried out in this direction, ranging from basic energy balance considerations of a sliding block to sophisticated models of granular flows over real topography including a variety of friction laws<sup>5–10</sup>. Readers can refer to a broad review already published<sup>11</sup>.

On the basis of the energy balance of a rigid sliding block, the Heim's ratio<sup>5</sup> (that is, the ratio of the drop height  $H$  to the runout distance  $\Delta L'$ ), is commonly used as an estimate of the effective friction coefficient. This ratio shows a clear decrease with increasing volume, raising two types of questions: (1) What is the physical meaning of the Heim's ratio? Does it really represent the effective friction during the landslide? If not, is the suggested volume dependence only an artefact of the use of the Heim's ratio instead of the effective friction? (2) Is there a more appropriate way to quantify the effective friction? Does it really decrease with increasing volume? If so, what is causing this volume dependence?

Here we address these questions with a focus on dense, catastrophic and rapid landslides. We first compile data on landslides from the literature and from our own analysis of remote-sensing data and confirm the common observation that the Heim's ratio decreases with increasing volume. We then develop an analytical relation between flow properties and the effective friction coefficient in a continuum model of granular column collapse over an inclined plane, and show that it generally differs from the Heim's ratio. On the basis of this analytical result, we develop consistent estimates of the effective friction coefficient of real landslides across the Solar System and find that friction decreases with increasing volume. We further confirm this scaling by a more complete approach, conducting simulations that account for topography and mass deformation to determine the friction coefficient that best reproduces the observed deposits of each landslide. These numerical simulations provide also estimates of landslide velocity, which indicate that the effective friction decreases with increasing velocity. We finally propose a single velocity-weakening friction law, inspired from concepts in earthquake physics (for example, flash heating of granular contacts), and incorporate it in our numerical models to show that it reproduces well the ensemble of observations of small to large landslides on Earth and other planetary surfaces.

## Results

**Heim's ratio for a large landslide data set.** We gathered a large collection of data on landslides on Earth (82) and other planetary bodies (89), including data from the literature and new data (42) obtained using existing digital topography models (DTM) or DTMs that we built ourselves for this purpose. Some examples are illustrated in Fig. 1. Our DTMs, based on the most accurate available imagery and state-of-the-art photogrammetry analysis tools (see Methods), all together provide the best data set presently available on planetary landslides (see Supplementary Table 1). Despite the great complexity and diversity of these landslides and the large dispersion in the data, a general relation between Heim's ratio and volume is clearly identified (Fig. 2a, see Supplementary Note 1 for the discussion on the origin of the Heim's ratio). Essentially,  $H/\Delta L' \sim 0.4\text{--}0.7$  for volumes smaller than  $10^6 \text{ m}^3$  and drops to values  $< 0.1$  for volumes  $> 10^9 \text{ m}^3$ . This has been previously observed and interpreted as a decrease of the effective friction coefficient as the volume increases<sup>5,8,12,13</sup>. The practical implication is that large landslides run over distances much longer than expected from the usual values of friction coefficient measured in laboratory experiments ( $\sim 0.6\text{--}0.7$ ). In this sense, large landslides are said to present high mobility or long runout distances<sup>5,6,8</sup>. However, as already long discussed in the literature, this interpretation is not as straightforward as it seems<sup>8,9,11,12,14,15</sup>. Confusion between the two independent questions formulated in the introduction has led some to refute the decrease of effective friction with volume because of the questionable meaning of the Heim's ratio<sup>15</sup>. Its limitations as a measure of the effective friction have long been recognized in the literature, based on the fact that its definition does not involve the displacement of the centre of gravity<sup>16</sup>, the spreading of mass or the role of the topography<sup>8,9,12,14,15</sup>. Regardless of the meaning of the Heim's ratio, a possible volume dependence of the effective friction coefficient remains to be properly established by taking into account the effects of mass deformation and topography, as will be demonstrated here.

**Effective friction from analytical description.** To advance our understanding of the mechanics of catastrophic landslides beyond the energy balance of a sliding block, and in particular to take into account the deformation of the mass, we consider here the collapse of a granular column over an inclined plane. This situation is simple enough to be amenable to an analytical solution, leading to a closed-form relationship between the Heim's ratio and the other parameters involved in the problem (friction coefficient, bed slope and initial dimensions of the mass). On the basis of an analytical solution of the one-dimensional thin-layer depth-averaged equations of mass and momentum conservation with a Coulomb friction law<sup>17–19</sup>, we derive the following relationship between the effective friction coefficient  $\mu_{\text{eff}}$  and the initial thickness of the released mass  $H_0$ , the slope  $\tan\theta$  and the distance travelled by the front along the slope  $\Delta L$  (see Supplementary Note 2 for the complete derivation and Fig. 2a for the definition of the parameters. Different geometries are illustrated in Supplementary Fig. 1):

$$\mu_{\text{eff}} = \tan\delta = \tan\theta + \frac{H_0}{\Delta L}. \quad (1)$$

The analytical solution also shows that the Heim's ratio is

$$\frac{H}{\Delta L'} = \tan\theta + \frac{1}{\cos^2\theta \left( \frac{2k}{\tan\delta - \tan\theta} + \frac{L_0}{H_0} - \tan\theta \right)}, \quad (2)$$

where  $L_0/H_0$  is the inverse of the initial aspect ratio and  $k$  an empirical coefficient (for example, with  $k=0.5$ , the results of granular collapse experiments are quantitatively reproduced<sup>4,20</sup>).

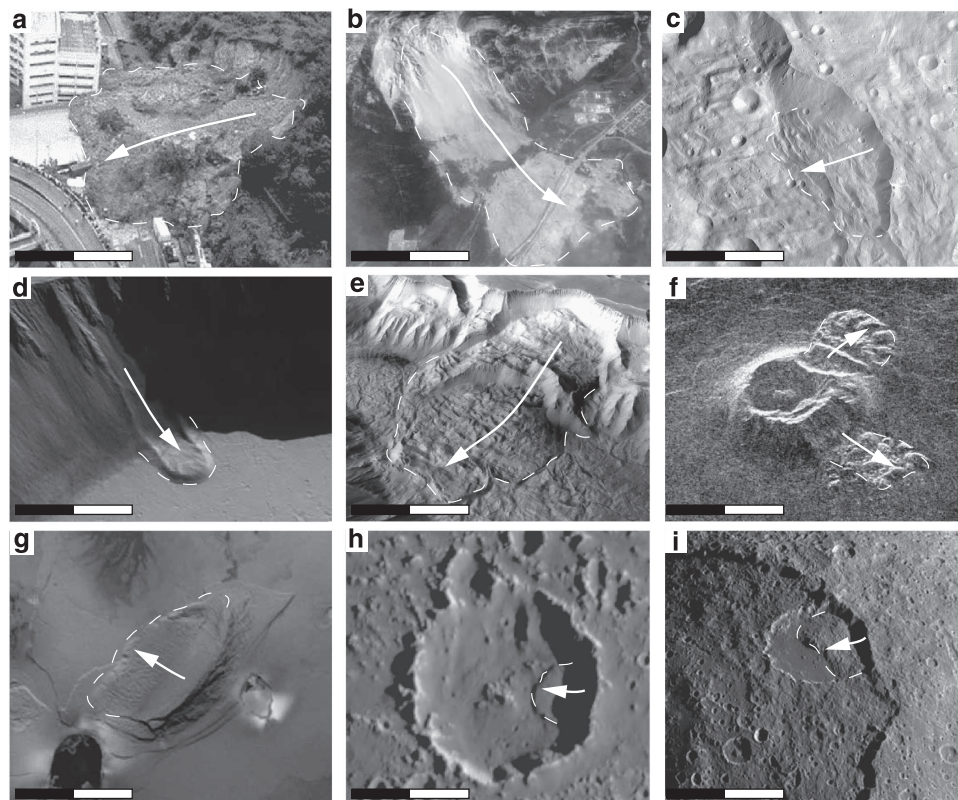


**Figure 1 | Examples of landslides observed in the Solar System.** Sizes range from tens of metres to hundreds of kilometres. On Earth: (a) Fei Tsui, Hong Kong (scale bar, 30 m); (b) Frank Slide, Canada (scale bar, 1 km). On Vesta (c) in the South pole region (scale bar, 80 km). On Mars: (d) Olympus Mons (scale bar, 2 km) and (e) Tithonium Chasma (scale bar, 10 km). On Venus: (f) in the Navka Region (scale bar, 25 km). On Jupiter's moons: (g) Euboea Montes on Io (scale bar, 100 km). (h) Inside Callisto's crater (scale bar, 10 km). On Saturn's moons: (i) Malun Crater on Iapetus (scale bar, 100 km). Deposits and sliding direction are highlighted with dashed white lines and arrows, respectively. Information on these landslides are reported in Supplementary Table 1.

Comparing equations (1) and (2), we observe that Heim's ratio results from a complex interplay between different quantities and differs significantly from the effective friction (details are provided in Supplementary Note 2). This is indeed confirmed by our observations (Fig. 3a). Equation (1) provides a more consistent estimate of the effective friction coefficient found from observations. We apply it to our data set and find that the effective friction clearly decreases with increasing volume whatever the planetary environment (Fig. 2c and see the subsection concerning application to real data in Supplementary Note 2). Combining laboratory and natural scale data (Fig. 2c), we find that the friction decreases for volumes larger than  $\sim 10^3 \text{ m}^3$ .

**Effective friction from numerical modelling.** The analytical approach does not account for the complex effect of the three-dimensional (3D) topography, which plays a key role in the landslide dynamics and deposits. Furthermore, the value of the effective friction coefficient derived from the analytic solution is mainly derived from the data on runout distance. We therefore assess here the ability of this empirical friction coefficient to explain the full extension of the deposits by simulating some landslides using the *SHALTOP*<sup>20–22</sup> numerical model that takes into account the real 3D topography. Although this model does not account for all the complex aspects of natural flows, such as the presence of heterogeneous materials (nature and size) or a fluid phase (gas or liquid) and the physical processes potentially acting during the flow (for example, fragmentation<sup>2</sup>, erosion/

deposition<sup>3,4</sup>), it represents a significant advance compared with simple analytical solutions or scaling laws because of its ability to account for topography effects and mass deformation.

For each landslide, we used *SHALTOP* simulations to determine by trial and error the friction coefficient  $\mu_s$  that best reproduces the deposit area inferred by satellite imagery analysis<sup>9,10</sup> (see Supplementary Fig. 6). We found that  $\mu_s$  was very similar (within  $3^\circ$ ) to the effective friction coefficient  $\mu_{\text{eff}}$  obtained from the analytical solution (Fig. 3b). Their difference is within the range induced by the uncertainty of the estimate of the initial scar geometry<sup>10</sup>. This is an important result for the calibration of numerical models, indicating that an estimate of the friction coefficient needed to simulate real landslides can be readily obtained from equation (1).

Many numerical studies have found friction coefficients similar to ours for landslides on Earth<sup>23–25</sup>. Discrete element modelling of large Martian landslides requires similar values of the friction coefficient<sup>26</sup>, showing that, whatever the type of model used, low friction is required to explain observations.

Numerical simulations also provide an estimate of the landslide velocity. The maximum velocity is known to be overestimated in depth-averaged thin layer models by only about 20% and the mean velocity is correctly estimated<sup>20,27,28</sup>. We calculate the mean velocity from the simulations by averaging the velocity in space and time over the whole landslide surface and duration. Velocities in our simulations agree with those reported for terrestrial landslides<sup>25</sup> (Fig. 4a). Dispersion in velocity values is expected given that topographic slopes over which landslides occur can vary from  $0^\circ$  to  $40^\circ$  locally as well as variousness in

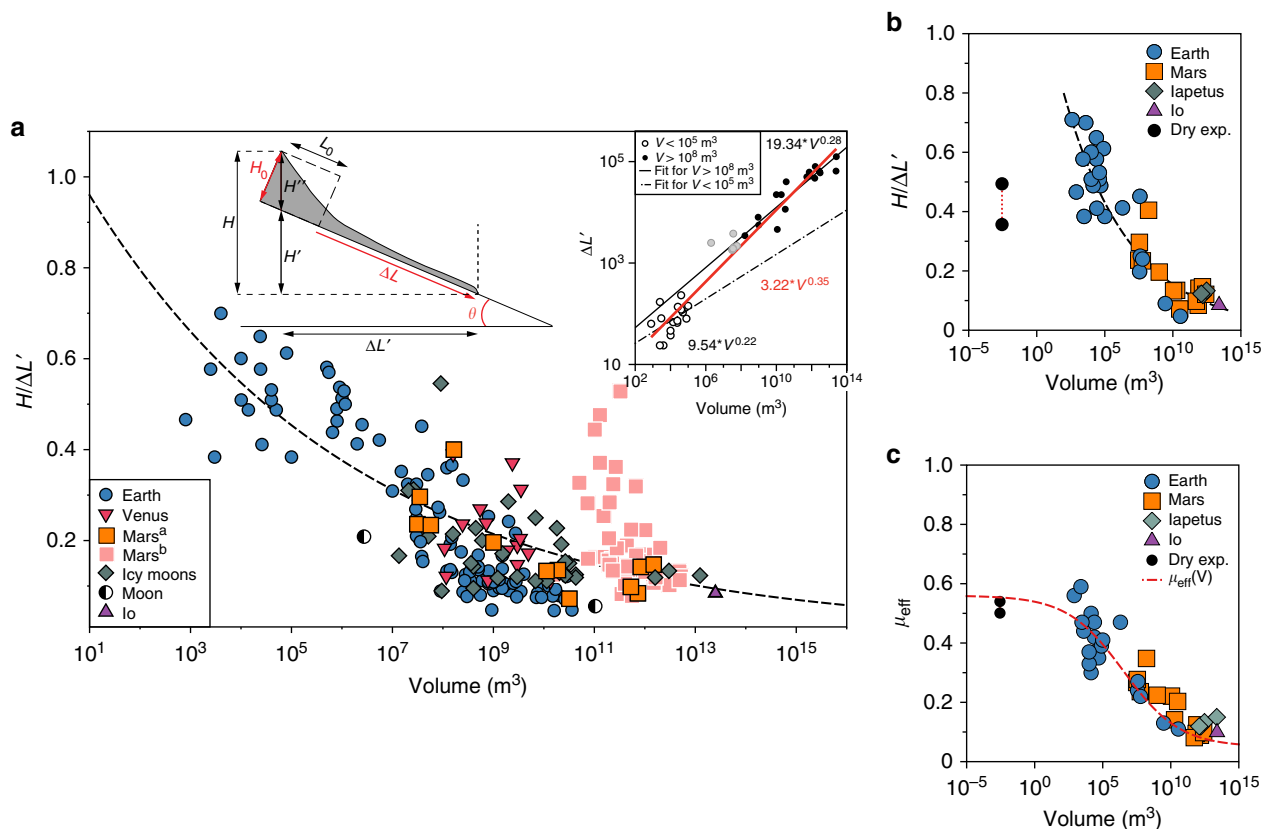


**Figure 2 | Heim's ratio and effective friction as a function of volume.** (a) Heim's ratio ( $H/\Delta L'$ ) for different planetary bodies: terrestrial data come from literature<sup>8,50,62</sup> (Blue bullet); Martian data (Mars<sup>a</sup>) come from the literature<sup>10</sup> and this study after stereo extraction from CTX and HRSC images (orange square); Martian data (Mars<sup>b</sup>) from previous work<sup>63</sup> (pink square); data for the Moon (half black circle) and icy moons including Rhea, Callisto and Iapetus (grey lozenge) are from the literature<sup>36,64</sup>; Io data are from the previous work<sup>65</sup> (purple triangle); Venus data come from a former study<sup>66</sup> (orange triangle). The dashed line is the best fit of Terrestrial, Martian<sup>b</sup> and Io data for which DTMs or accurate field data<sup>62</sup> are available (symbols with thick outlines):  $H/\Delta L' = 1.2 \times V^{-0.089}$ . Owing to the absence of accurate DTMs, volume of landslides on the Moon, Venus and icy moons are estimated from the empirical relationship  $\Delta L'(V)$  derived from terrestrial data shown in the right inset. Metrics are defined by the sketch. (b) ( $H/\Delta L'(V)$ ) and (c) ( $\mu_{eff}(V)$ ) for constrained landslides on Earth, Mars, Iapetus and Io. Experimental results<sup>4</sup> (black plain circle). The dashed red curve is the prediction from the final velocity-dependent law fitted to the terrestrial values including experimental results. All the values of panels b and c are reported in Supplementary Table 1. The data follows a trend  $\mu_{eff} \sim V^{-0.0774}$  for volumes larger than  $\sim 10^3 m^3$ . The scatter of the data for  $\mu_{eff}(V)$  in c is significantly smaller than for  $H/\Delta L'(V)$  in b (see statistics in Supplementary Table 4). For the sake of clarity, error bars are not shown but are approximately the size of each symbol on the horizontal axis and twice this size on the vertical axis.

materials involved. Experimental work<sup>4</sup> has shown that the mean velocity is  $\sim 2.5$  times greater on a slope of  $22^\circ$  than that on a flat bottom. Although new constraints on landslide velocities on Earth are emerging from seismological observations<sup>28,29</sup> and from a few rock avalanches that have been observed and/or filmed *in situ*<sup>25</sup>, the simulation approach adopted here is the only way to quantitatively recover landslide velocities for remote and past events on Earth and beyond.

We find that the landslide velocity increases with the volume of the released mass (Fig. 4a). Hence, the volume dependence of  $\mu_{eff}$  can be interpreted as a velocity dependence of friction, which is a more usual representation to investigate frictional weakening in solid mechanics and earthquake physics. Figure 4b shows that the effective friction decreases as a function of velocity. This general trend, observed for all landslides studied here, suggests a common mechanism that induces frictional weakening at increasing flowing velocities.

**Quantification of frictional weakening.** While several processes may lead to friction reduction under certain conditions<sup>2-4,8,12,24,30-37</sup> (see Supplementary Discussion), it is not

clear if the observations can be explained by a single process or if different processes act at different scales or in different environments. To clarify this, we need to quantify these potential processes and assess their compatibility with observations and environmental conditions. As a first step in this direction, our aim is to identify empirical friction laws that provide a unifying framework to explain the landslide scaling observations across all planetary environments (for example, low gravity, airless environment and absence of water table). The challenge will then be to quantitatively compare this empirical friction law to the mechanical behaviour derived from a specific mechanism.

Here we investigate quantitatively the compatibility between our observations of catastrophic landslides and two weakening mechanisms that have been introduced in very different contexts and for which constitutive relationships are available in a form that enables comparison with our results on real landslides. These relationships are (i) a friction law controlled by flash heating proposed to explain frictional weakening during earthquakes<sup>32,38</sup> and (ii) a rheology law proposed to describe laboratory granular flows<sup>39</sup>.

Frictional weakening with increasing slip velocity has been invoked to explain key features of earthquakes<sup>40</sup> and has been



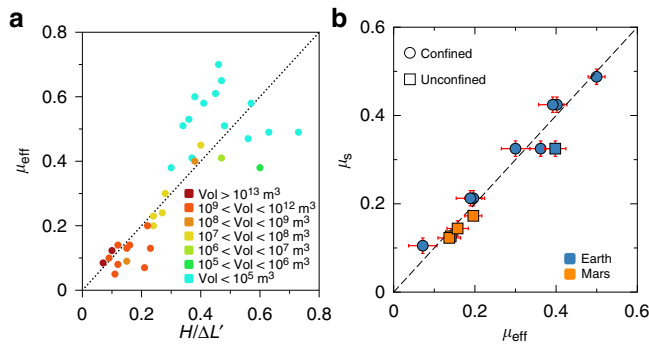


**Figure 3 | Heim's ratio, analytical effective friction and friction derived from simulations.** (a) Comparison between  $\mu_{\text{eff}}$  and  $H/\Delta L'$ . Each landslide is represented by a circle the colour of which is related to its volume. The dotted line represents  $x = y$ , where  $x$  and  $y$  are the abscissa and ordinate, respectively. (b) The friction coefficient  $\mu_s$  calibrated in the numerical modelling to reproduce the observed extension of the deposits is comparable to the effective friction coefficient  $\mu_{\text{eff}}$  estimated from natural data using the simple analytical formula (1). Error bars in panel b represent the uncertainties in the estimation of  $\mu_{\text{eff}}$  and uncertainties of  $\mu_s$  calibrated by trial and error. For the sake of clarity, error bars are not shown on panel a but are approximately twice the size of each symbol.

observed in laboratory experiments of fast sliding on rocks and gouge materials<sup>41</sup>. A micro-mechanical process that can lead to dramatic velocity-weakening is flash heating<sup>32,38</sup>. The real contact between two rough solid surfaces generally occurs over a small fraction of their nominal contact area, on highly stressed micro-contacts (asperities). Slip produces frictional heating at the micro-contact scale. If slip is fast enough to prevent heat dissipation by conduction, the micro-contact experiences a significant transient temperature rise that activates thermal effects such as melting, dehydration and other phase transformations. This reduces the local shear strength of the micro-contact and leads to a macroscopic decrease of the friction coefficient as a function of sliding velocity. Laboratory observations of velocity-weakening have been previously interpreted within the framework of flash heating for rock sliding<sup>38,42</sup> and granular flows<sup>43</sup>. Owing to its microscopic scale and effects, application of flash heating to a very rough, irregular and/or heterogeneous surface where material in contact can be different and the shear zone not well defined is still valid and thus suitable for landslides. Conceivably, flash heating may occur at the inter-granular contact level during a landslide, a point that we will discuss more quantitatively below.

The applicability of these concepts to icy moons<sup>44</sup> is essentially speculative as the behaviour of icy grounds on planetary bodies remains a very unconstrained problem. Theoretical and experimental studies<sup>45–47</sup> have shown that similar behaviour can be observed for water ice at low temperatures and for rocky materials, suggesting that flash heating might occur on ice<sup>48</sup>. However, quantitative differences between planetary bodies similar to the variability observed between different rocky materials on Earth is expected. Because this is a very unconstrained topic, our approach here is only a first-order analysis<sup>36</sup>.

Basic flash weakening theory<sup>32,38</sup> yields the following compact form to describe the steady-state friction coefficient as a function of slip velocity  $U$ : if  $\|U\| > U_w$

$$\mu(U) = \frac{\mu_o - \mu_w}{\|U\|/U_w} + \mu_w, \quad (3)$$

otherwise,

$$\mu(U) = \mu_o, \quad (4)$$

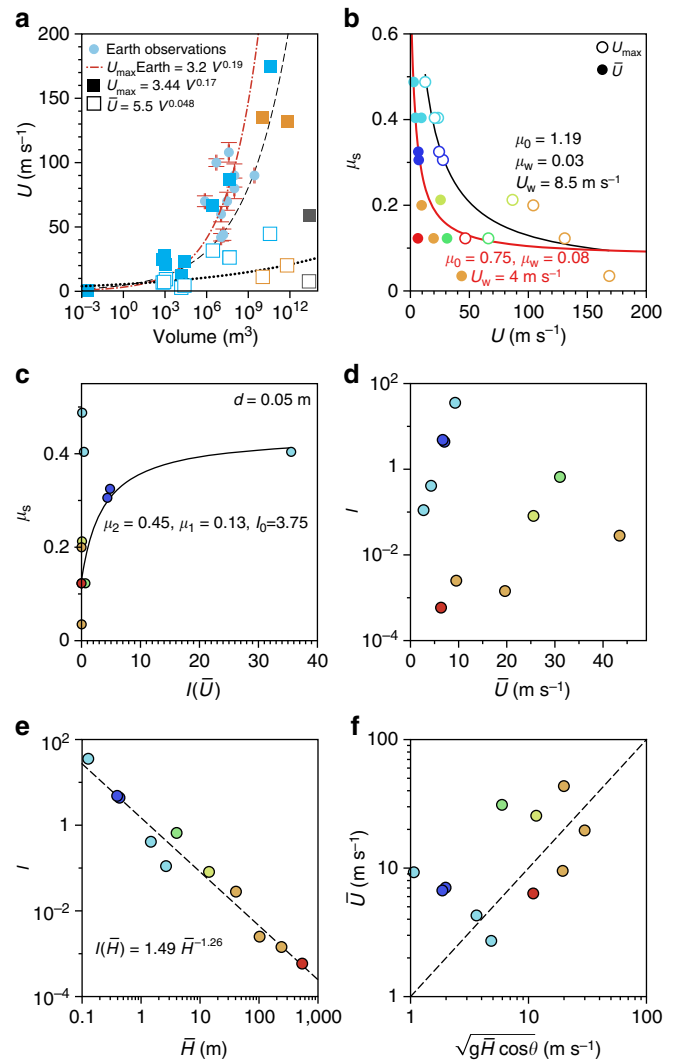


**Figure 4 | Frictional and dynamic properties from simulations.** (a) Mean (that is, spatially and temporally integrated) and maximum velocities calculated in the simulation of real landslides over 3D topography as a function of the volume. Colours correspond to Earth in blue, Mars in orange and Iapetus in grey. Circle symbols represent measurements of maximum velocity (and their respective uncertainties) from terrestrial landslides reported in the literature<sup>25</sup>. The red dash-dotted curve is the best fit for all terrestrial data (simulations and reported values). Black dash-dotted lines are the best fit of the maximum and mean velocities, respectively, obtained from simulations of landslides on Earth, Mars and Iapetus. (b,c) The calibrated friction coefficient  $\mu_s$  as a function of (b) the flow velocity and (c) the inertial number calculated from equation (5). Equation (8) is fitted to the maximum velocity (values in black) and to the mean velocity (values in red). (d,e) Inertial number as a function of (d) the mean velocity and (e) the mean thickness. (f) Mean velocity as a function of  $\bar{v}_f = \sqrt{g\bar{H}\cos\theta}$ , where  $\bar{H}$  is the mean thickness during the flow and  $\theta$  the mean slope (dashed line is equality). The best fits are displayed except for d and f. Colour scale indicating volumes, that is, cool colours for small volumes, warm colours for large volumes as for Fig. 3a except for panel a for which colours correspond to the planetary body as mentioned in the legend. For the sake of clarity, error bars are not shown but are approximately the size of each symbol.

where  $\mu_o$  and  $\mu_w$  are the static and thermally weakened friction coefficients, respectively, and  $U_w$  is a characteristic velocity for the onset of dramatic weakening, controlled by competition between

frictional heating and heat conduction (see Supplementary Discussion). Even though natural landslides could span a broad range of parameters  $\mu_o$ ,  $\mu_w$  and  $U_w$ , we found that equations (3) and (4) with a single set of parameters are consistent with the whole set of friction coefficients and velocities obtained in our simulations of real landslides (Fig. 4b). The best fitting parameters are  $\mu_o = 0.75$ ,  $\mu_w = 0.08$  and  $U_w = 4 \text{ m s}^{-1}$ .

In order to investigate the effect of velocity-weakening friction on landslide dynamics, we introduced the friction law (3) with the global best fitting parameters in the *SHALTOP* numerical model. We then simulated natural landslides over 3D topography for several examples on Earth, Mars and Iapetus following previous works<sup>9,10</sup>. Without any further calibration, we were able to reproduce the observed runout distance and the shape of the deposit with errors below 12%. We then determined a set of parameters that provided the best global agreement between simulations and observations for all the tested cases:  $\mu_o = 0.84$ ,  $\mu_w = 0.11$ ,  $U_w = 4.1 \text{ m s}^{-1}$  (details on the simulations are given in Supplementary Methods and Supplementary Figs 8 and 9). Results from a simulation with velocity-dependent friction are shown in Fig. 5. The friction coefficient fluctuates in space and time during the landslide: fast flowing regions experience friction as low as  $\mu_w$  while slow flowing regions experience friction as high as  $\mu_o$ . The runout distances are then reproduced with an error <8%. The morphology of the deposit is also well reproduced. This shows that a single set of friction parameters can reproduce first- and second-order features of landslides with volumes varying by up to 14 orders of magnitude.

Note that when the threshold in equation (3) is not used in the simulation, the deposit area is affected by <12% and the runout distance by <8%. The distribution of the velocity and hence the thickness is slightly affected, especially at the beginning of the event ( $t < 0.3t_f$ ), but solutions tend to converge towards the end of the simulation. The mean velocities calculated with the velocity-weakening friction law (3) are similar to the velocities obtained using a constant friction law with the friction coefficient  $\mu_s$  fitted to reproduce the deposit. However, strong differences in the local

velocity field and thickness are observed between these two types of simulations.

Because of the large variability of the materials involved in the different landslides, we also varied the parameters of equation (3) to maximize the agreement between simulation and observations for each example individually. The parameters that best reproduce the deposits of studied landslides fall in the following ranges:  $\mu_o \in [0.5-0.96]$ ,  $\mu_w \in [0.08, 0.16]$  and  $U_w \in [0.8-5.2] \text{ m s}^{-1}$ . These values are comparable to the range derived from laboratory experiments<sup>32</sup> (where  $\mu_o \in [0.6-0.88]$ ;  $\mu \in [0.12-0.16]$  and  $U_w \in [0.1-0.3] \text{ m s}^{-1}$ ). The main difference is observed for  $U_w$ , which might be explained by the different conditions prevailing in landslides, that is, granular material, lower confinement stress (e.g. see also Supplementary Tables 2 and 3).

Note that small-scale laboratory experiments of granular collapse are well reproduced by finite-element numerical models using a Coulomb friction law with a constant friction coefficient<sup>49</sup>. Experimental studies<sup>4</sup> show that granular collapse over beds with slope angles up to  $22^\circ$  have a maximum velocity of about  $2 \text{ m s}^{-1}$ , that is,  $< 4 \text{ m s}^{-1}$ , so that equation (3) predicts a constant  $\mu = \mu_o$ . The characteristics of natural rockfalls from  $1$  to  $10^3 \text{ m}^3$  can be reproduced with a constant friction coefficient<sup>50</sup>. If we use our scaling law between volume and initial thickness of the released mass (see Supplementary Equation (20) in Supplementary Note 2 and Supplementary Note 1), a volume of  $10^3 \text{ m}^3$  would correspond to  $H_0 \simeq 2.8 \text{ m}$ . Granular collapse experiments<sup>4,51</sup> show that the maximum velocity is a function of  $\sqrt{gH_0 \cos \theta}$ . As a result, on slope angles  $\theta \simeq 30^\circ$  typical for these rockfalls, the threshold velocity would be higher than  $4.8 \text{ m s}^{-1}$ . All these simple calculations are in very good agreement with the empirical parameters of the friction laws (3) and (4).

Rheological laws for granular materials have been proposed in which the friction coefficient depends on the so-called inertial number<sup>39,52,53</sup>,

$$I = \frac{\dot{\gamma}d}{\sqrt{P/\rho_s}} \quad (5)$$

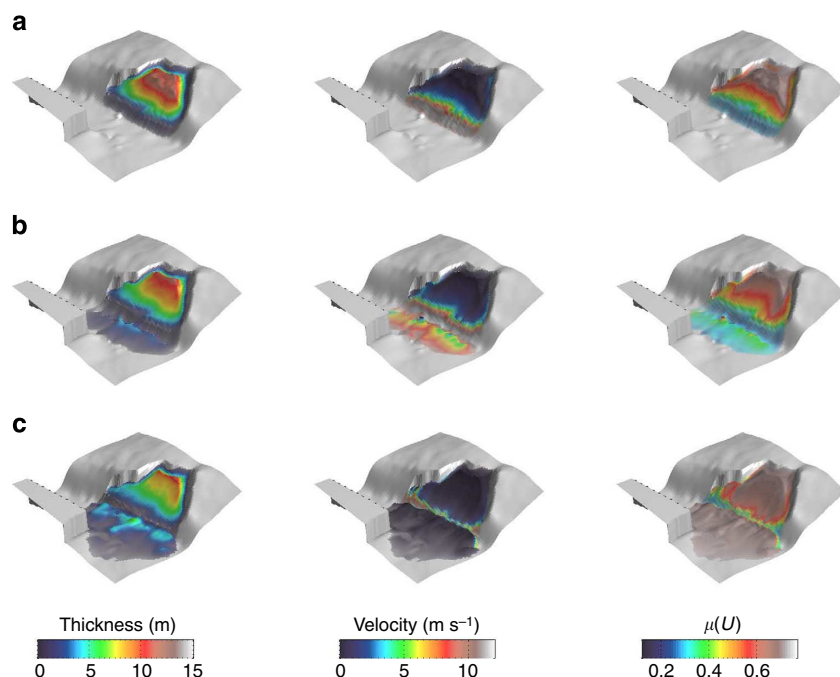


**Figure 5 | Fei Tsui (Hong Kong) landslide is simulated with the velocity-weakening friction law.** Thickness, velocity and friction coefficient are shown at three different times during the flow (that is, (a) 1 s, (b) 3 s and (c) 9 s). Friction weakening derived from equation (8) with  $\mu_o = 0.84$ ,  $\mu_w = 0.11$  and  $U_w = 4.1 \text{ m s}^{-1}$  has been used here. The example refers to Fig. 1a.

where  $\dot{\gamma}$  is the shear strain rate,  $d$  the particle diameter,  $P$  the confining stress and  $\rho_s$  the particle density. Assuming hydrostatic pressure  $P = \rho_s g H \cos \theta$  and  $\dot{\gamma} \simeq U/H$ , where  $g$  is the gravitational acceleration,  $H$  the thickness during the flow,  $\theta$  the mean slope along the landslide path and  $U$  the mean velocity, we obtain

$$I \simeq \frac{Ud}{H\sqrt{gH\cos\theta}} \quad (6)$$

If we replace the velocity and thickness by their values averaged over space and time for each landslide, we find that, in the simulations with a constant friction coefficient,  $\mu_s$  increases as  $I$  increases (Fig. 4c).

On the basis of laboratory experiments, the following friction law for dense granular flows has been introduced<sup>39</sup>:

$$\mu(I) = \frac{\mu_2 - \mu_1}{(1 + I_0/I)} + \mu_1 \quad (7)$$

The parameters that best fit our simulation results are  $\mu_1 = 0.13$ ,  $\mu_2 = 0.45$  and  $I_0 = 3.75$ , assuming  $d = 0.05$  m (Fig. 4c). For reference, the following parameters from laboratory experiments have been obtained<sup>39</sup>:  $\mu_1 = 0.36$ ,  $\mu_2 = 0.62$  and  $I_0 = 0.279$ . We implemented equation (7) in the SHALTOP model. Simulations adopting the best global fitting parameters obtained from Fig. 4c failed to reproduce the observed deposits. By tuning the parameters for each case individually, we were able to satisfactorily reproduce the runout distance but not the morphology of the deposits.

### A multiscale phenomenological friction law for granular flows.

We will now consider the similarities between the two friction laws described above (equations (3) and (7)). The flash heating friction law (equation (3)) features velocity-weakening that is a function of  $1/U$  at large velocities. Granular shear laboratory experiments with specified thicknesses generally present velocity-strengthening behaviour consistent with equation (7). However, in our simulations the flow thickness is unconstrained and we find that, in contrast to what is first expected from equation (6), the inertial number  $I$  does not increase systematically with velocity  $U$  (Fig. 4d). We find that  $I$  is mainly controlled by  $\bar{H}$ ; (Fig. 4e). This is related to a very rough scaling found here between  $\bar{U}$  and  $\sqrt{g\bar{H}\cos\theta}$  (Fig. 4f). Assuming the same relationship for non-averaged values of  $U$  and  $H$ , taken literally, would lead to  $I \propto 1/H$  or, equivalently, to  $I \propto 1/U^2$ . As a result, the granular friction law (equation (7)) also leads to velocity-weakening, with an asymptotic behaviour of the form  $1/U^2$  at high velocities. Note that  $\mu \propto U^{-0.5}$  has been reported for water ice<sup>47</sup>. This suggests that velocity-weakening with asymptotic behaviour of the power-law form  $1/U^n$  may be compatible with landslide observations and our current analysis favours an exponent  $n$  closer to 1 than to 2. Although both friction laws lead to qualitatively similar (power-law) velocity-weakening behaviour, quantitative differences in their velocity-weakening exponent make the flash heating law suitable for reproducing landslides, over a wide range of volumes and planetary environments, but not the granular flow law.

Our study suggests that a universal velocity-weakening friction law can describe small to large catastrophic landslides occurring in natural environments on Earth and other planetary bodies. Essentially, the friction coefficient is required to vary from around  $\mu_l = 0.7$  (a friction angle of  $\delta \simeq 35^\circ$ ) for low velocity flows to values as small as  $\mu_r = 0.1$  ( $\delta_r = 5.7^\circ$ ) for rapid flows. The nature of the materials involved is expected to add scatter to these values. Typically, spherical beads used in laboratory experiments<sup>39</sup> have friction coefficients of around 0.65, while friction coefficients of natural rocks may reach 0.6–0.7 and even 0.7–0.75 for low-

temperature water ice<sup>45</sup> relevant for icy moons. On the basis of the foregoing discussion, we propose the following friction law:

$$\mu(U) = \frac{\mu_o - \mu_w}{(1 + \|U\|/U_w)} + \mu_w, \quad (8)$$

with  $\mu_o = 0.84$ ,  $\mu_w = 0.11$  and  $U_w = 4 \text{ m s}^{-1}$ . Including a sharp velocity threshold as in equations (3) and (4) does not significantly affect the results of our landslide simulations. Even though this friction law is similar to the one derived from flash heating theory, the physical weakening process controlling landslides could be different. Indeed, the value of  $U_w$  found here is an order of magnitude higher than in solid friction experiments<sup>54</sup>. While this can be interpreted as a macroscopic velocity distributed over a granular shear zone a few tens of particles thick, there is evidence that inter-granular slip activity is highly intermittent<sup>55</sup> resulting in inter-particle velocities comparable to or faster than the macroscopic velocity<sup>32</sup>.

An intuitive explanation of this velocity-weakening is that, whatever the scale, higher velocities increase the fluctuations in granular flows and may locally decrease the volume fraction, possibly decreasing frictional dissipation and enabling more complex flows (vortices and so on). Indeed, recent discrete element modelling of dry granular flows highlights the appearance of possible regimes dominated by large-scale vortices, significantly reducing the effective friction<sup>56</sup>, although this remains to be observed in laboratory experiments. Different mechanisms may also be responsible for this friction weakening, owing to the great complexity of natural landslides that involve very different material properties (for example, composition and strength), environment variables (for example, air pressure and gravity) and physical processes at play (for example, fluid/grain interactions and erosion/deposition processes). Rock friction experiments showing a similar velocity-weakening behaviour have also been associated with a multitude of physical processes<sup>54</sup> (note that equation (8) can be used to fit these experiments, see Supplementary Fig. 7). Finally, we were able to obtain a predictive curve from the velocity-dependent friction by returning the relationship between velocity and volume (see  $U_{\text{max,earth}}$  on Fig. 5a) into equation (8) as shown in Fig. 2c. The best fit on the terrestrial data (that is, including experimental results) is obtained for  $\mu_o = 0.56$ ,  $\mu_w = 0.05$ ,  $U_w = 4$  and  $U = 0.17 \text{ V}^{0.21}$  with a coefficient of determination  $R^2 = 0.90$ . Nevertheless, variations of these parameters are expected for each individual landslide as mentioned previously.

### Discussion

Using a large range of well-constrained data on landslides observed on different planets, an analytical solution of dry granular flows and numerical modelling over realistic 3D topography, we have demonstrated that the classically used Heim's ratio is not equal to the effective friction acting on landslides. We propose a more accurate way to quantify this effective friction based on field observations or remote-sensing data. As previously observed for the Heim's ratio and despite the large variety of landslide environments examined here, a clear decrease of the effective friction with increasing volume of the released mass is found while accounting for the deformation of the sliding mass and the 3D topography.

The novelty in our study is the correlation between the sliding velocity and the volume. The observed decrease of the friction coefficient with volume can be interpreted as velocity-dependent frictional weakening. Comparing numerical models of natural landslides on real 3D topography to field data on their deposits, we find an empirical relationship between the effective friction and the flow velocity. This relationship is surprisingly similar to a friction law derived for weakening by flash heating. The resulting friction



coefficient varies from high values, up to  $\mu_o = 0.7\text{--}0.8$ , at low velocities (that is, small volumes) to very small values, down to  $\mu_w < 0.1$ , for rapid flows (that is, large volumes). Simulations of natural landslides based on this empirical friction law, with a single set of parameters, reproduce the observed landslide deposits with good accuracy over a very broad range of volumes and contexts. In contrast, we find that a friction law derived from laboratory experiments of granular flows is not compatible with natural observations.

Although our analysis cannot determine the physical origin of frictional weakening in landslides, we propose here a velocity-weakening friction law capable of describing, under a unifying phenomenological framework, the behaviour of small to large landslides observed on different planetary bodies.

## Methods

**Analytical solution.** The analytical solution was developed on the basis of various studies<sup>17–19</sup> and describes the collapse over an inclined plane of a granular mass of effective friction coefficient  $\mu_{\text{eff}} = \tan\delta$ , where  $\delta$  is the effective friction angle of the granular material. This solution is derived from the one-dimensional thin-layer depth-averaged equations of mass and momentum conservation with a Coulomb friction law, using the method of characteristics<sup>17,19</sup> (see Supplementary Notes 1 and 2).

**Landslide identification and topographic reconstruction.** For geomorphic measurements and numerical simulations, the initial scar geometry, the shape of the initial released mass and the bottom topography were reconstructed from observations using remote-sensing data in order to identify the landslide deposits in optical and elevation data. Landslides were identified using imagery provided by the Planetary Data System from the Mars Reconnaissance Orbiter, Mars Express, Cassini and Galileo missions. We produced the digital elevation models by photogrammetry based on rigorous sensor models from which ephemeris (that is, SPICE kernels) were extracted from the USGS ISIS software distribution<sup>57</sup> (Integrated Software for Imagers and Spectrometers) and the NASA Ames StereoPipeline<sup>58</sup> for data from the Cassini and Galileo missions. For the Mars Reconnaissance Orbiter cameras (HiRISE and CTX), DTM extraction was carried out on our photogrammetry workstation using the SOCET SET commercial software suite from BAE Systems. Bundle adjustments were performed for all of our examples in order to minimize errors due to uncertainties on SPICE kernels. In order to provide a realistic bottom topography, we reconstructed the initial mass released using geographic information system applications as already described<sup>10,59</sup> (see Section 4.2.2 of previous study<sup>10</sup>) and performed previously<sup>9,10,27,59</sup>.

**Numerical simulations.** The simulations were performed using the *SHALTOP* model<sup>20,21</sup> based on the thin layer approximation for the depth-averaged equations of mass and momentum conservation with a Coulomb friction law. This model has been successfully applied to the modelling of laboratory experiments and natural examples<sup>9,10,20,21,27–29,50,60</sup>. Comparison with experiments of granular collapse and with discrete element models<sup>20,61</sup> shows that thin-layer models adequately reproduce the deposit and the overall dynamics for aspect ratios  $a < 1$ . This is the case for all the landslides for which we have a DTM and detailed field data (see Supplementary Table 1). Although the driving forces are overestimated in thin layer depth-averaged models, leading to overestimates of the initial velocity by up to 20% for aspect ratios  $a \approx 1$  the deposits are correctly reproduced. Recent simulation of the seismic waves generated by the flow along the topography and comparison with seismic records suggest that the landslide dynamics are also well reproduced by these numerical models<sup>28,29,50</sup>.

For each landslide, we calibrated the effective friction coefficient of the simulation,  $\mu_s = \tan\delta$ , in order to best fit the deposit area observed from the field and/or satellite imagery analysis<sup>9,10,27–29,60</sup>. Note that using only one empirical parameter ( $\mu_s$ ), these models reproduce the whole deposit extension and even its general mass distribution quite well over a wide range of conditions (Supplementary Fig. 6). Here, we also integrated the new rheological laws into the model as shown in Fig. 5 and Supplementary Fig. 8.

**Sensitivity of the results.** The impact of the DTM resolution has already been discussed in former studies<sup>10,27</sup>. Reducing the spatial resolution of the DTM by a factor of two leads to an error of about 3° on the friction angle. When necessary, the topographic grid is oversampled in order to converge in terms of spatial resolution. In order to reconstruct the pre-failure and bottom topographies, we used the method previously developed<sup>10</sup> which has been shown to be efficient and lead to small error on the derived friction coefficient from numerical modelling (see Section 4.2 of ref. 10). As shown previously, the runout distance is weakly affected by the geometry of the initial scar geometry<sup>10</sup>. This leads to uncertainties

in the estimation of the friction angle  $\delta$  of about 3° (Fig. 3b). The DTM resolutions are good enough to not affect our results in this 1-sigma band.

## References

- Otto, A. *et al.* Mass-wasting features and processes in Vesta's south polar basin Rheasilvia. *J. Geophys. Res. Planets* **118**, 2279–2294 (2013).
- Davies, T. R., McSaveney, M. J. & Hodgson, K. A. A fragmentation spreading model for long-runout rock avalanches. *Can. Geotech. J.* **36**, 1096–1110 (1999).
- Mangeney, A., Tsimring, L. S., Volfson, D., Aranson, I. S. & Bouchut, F. Avalanche mobility induced by the presence of an erodible bed and associated entrainment. *Geophys. Res. Lett.* **34**, L22401 (2007).
- Mangeney, A. *et al.* Erosion and mobility in granular collapse over sloping beds. *J. Geophys. Res.—Earth Surf.* **115**, F03040 (2010).
- Heim, A. *Bergsturz und Menschenleben* (Fretz and Wasmuth, 1932).
- Dade, W. B. & Huppert, H. E. Long-runout rockfalls. *Geology* **26**, 803–806 (1998).
- Pouliquen, O. Scaling laws in granular flows down rough inclined planes. *Phys. Fluids* **11**, 542–548 (1999).
- Legros, F. The mobility of long-runout landslides. *Eng. Geol.* **63**, 301–331 (2002).
- Lucas, A. & Mangeney, A. Mobility and topographic effects for large valles marineris landslides on Mars. *Geophys. Res. Lett.* **34**, L10201 (2007).
- Lucas, A., Mangeney, A., Mège, D. & Bouchut, F. Influence of the scar geometry on landslide dynamics and deposits: application to martian landslides. *J. Geophys. Res.—Planets* **116**, E10001 (2011).
- Pudasaini, S. P. & Hutter, K. *Avalanche Dynamics: Dynamics of Rapid Flows of Dense Granular Avalanches* (Springer, 2007).
- Davies, T. R. Spreading of rock avalanche debris by mechanical fluidization. *Rock Mech.* **15**, 9–24 (1982).
- Hayashi, J. N. & Self, S. A comparison of pyroclastic flow and debris avalanche mobility. *J. Geophys. Res.* **97**, 9063–9071 (1992).
- Campbell, C., Clearly, P. W. & Hopkins, M. Large-scale landslide simulations: Global deformation, velocities and basal friction. *J. Geophys. Res.* **100**, 8267–8283 (1995).
- Staron, L. & Lajeunesse, E. Understanding how volume affects the mobility of dry debris flows. *Geophys. Res. Lett.* **36**, L12402 (2009).
- Hungr, O. Mobility of rock avalanches. *Report of the National Research Institute for Earth Science and Disaster Prevention, Tsukuba, Japan* **46**, 11–20 (1990).
- Mangeney, A., Heinrich, P. & Roche, R. Analytical solution for testing debris avalanche numerical models. *Pure Appl. Geophys.* **157**, 1081–1096 (2000).
- Kerswell, R. R. Dam break with Coulomb friction: a model of granular slumping? *Phys. Fluids* **17**, 057101 (2005).
- Faccanoni, G. & Mangeney, A. Exact solution for granular flows. *Int. J. Num. Anal. Meth. Goemach.* **37**, 1408–1433 (2013).
- Mangeney-Castelnau, A. *et al.* On the use of Saint-Venant equations to simulate the spreading of a granular mass. *J. Geophys. Res.* **110**, B09103 (2005).
- Mangeney, A., Bouchut, F., Thomas, N., Vilotte, J.-P. & Bristeau, M. O. Numerical modeling of self-channeling granular flows and of their levee-channel deposits. *J. Geophys. Res.* **112**, F02017 (2007).
- Farin, M., Mangeney, A. & Roche, O. Fundamental changes of granular flow dynamics, deposition and erosion processes at high slope angles: insights from laboratory experiments. *J. Geophys. Res.* doi:10.1002/2013JF002750 (2013).
- Hungr, O., Dawson, R., Kent, A., Campbell, D. & Morgenstern, N. R. Rapid flow slides of coal-mine waste in British Columbia, Canada. *GSA Rev. Eng. Geol.* **15**, 191–208 (2002).
- Hungr, O. & Evans, S. G. Entrainment of debris in rock avalanches: an analysis of a long runout mechanism. *Bull. Geol. Soc. Am.* **116**, 1240–1252 (2004).
- Sosio, R., Crosta, G. B. & Hungr, O. Complete dynamic modeling calibration for the Thurwieser rock avalanche (Italian Central Alps). *Eng. Geol.* **100**, 11–26 (2008).
- Smart, K. J., Hooper, D. & Sims, D. Discrete element modeling of landslides in Valles Marineris, Mars. *AGU Fall Meeting. Abstract P51B-1430* (2010).
- Lucas, A., Mangeney, A., Bouchut, F., Bristeau, M. O. & Mège, D. in *Proceedings of the 2007 International Forum on Landslide Disaster Management* (eds Ho, K. & Li, V.) (International Forum on Landslide Disaster Management, Hong Kong, 2007).
- Favreau, P., Mangeney, A., Lucas, A., Crosta, G. & Bouchut, F. Numerical modeling of landquakes. *Geophys. Res. Lett.* **37**, L15305 (2010).
- Moretti, L. *et al.* Numerical modeling of the Mount Steller landslide flow history and of the generated long period seismic waves. *Geophys. Res. Lett.* **39**, L16402 (2012).
- Melosh, H. J. Acoustic fluidization: a new geologic process? *J. Geophys. Res.* **84**, 7513–7520 (1979).
- Eisemann, T. Mechanisms of large landslides. *Rock Mech.* **12**, 15–46 (1979).



32. Rice, R. J. Heating and weakening of faults during earthquake slip. *J. Geophys. Res.* **111**, B05311 (2006).
33. Goren, L. & Aharonov, E. Long runout landslides: the role of frictional heating and hydraulic diffusivity. *Geophys. Res. Lett.* **34**, L07301 (2007).
34. De Blasio, F. V. Landslides in Valles Marineris (Mars): a possible role of basal lubrication by sub-surface ice. *Planet. Space Sci.* **59**, 1384–1392 (2011).
35. Viesca, R. & Rice, J. R. Nucleation of slip-weakening rupture instability in landslides by localized increase of pore pressure. *J. Geophys. Res.* **B3**, 2156–2202 (2012).
36. Singer, K., McKinnon, W., Schenk, P. & Moore, J. Massive ice avalanches on Iapetus caused by friction reduction during flash heating. *Nat. Geosci.* **5**, 574–578 (2012).
37. Pudasaini, S. P. & Miller, S. A. The hypermobility of huge landslides and avalanches. *Eng. Geol.* **157**, 124–132 (2013).
38. Beeler, N. M., Tullis, T. E. & Goldsby, D. L. Constitutive relationships and physical basis of fault strength due to flash heating. *J. Geophys. Res.* **113**, B01401 (2008).
39. Jop, P., Forterre, Y. & Pouliquen, O. A constitutive law for dense granular flows. *Nature* **441**, 727–730 (2006).
40. Heaton, T. H. Evidence for and implications of self-healing pulses of slip in earthquake rupture. *Phys. Earth. Planet. Inter.* **64**, 1–20 (1990).
41. Tsutsumi, A. & Shimamoto, T. High velocity frictional properties of gabbro. *Geophys. Res. Lett.* **24**, 699–702 (1997).
42. Goldsby, D. L. & Tullis, T. E. Flash heating leads to low frictional strength of crustal rocks at earthquake slip rates. *Science* **334**, 216–218 (2011).
43. Kuwano, O. & Hatano, T. Flash weakening is limited by granular dynamics. *Geophys. Res. Lett.* **38**, L17305 (2011).
44. Lucas, A. Slippery sliding on icy Iapetus. *Nat. Geosci.* **5**, 524–525 (2012).
45. Beeman, M., Durham, W. B. & Kirby, S. H. Friction of ice. *J. Geophys. Res.* **93**, 7625–7633 (1988).
46. Miljković, K., Mason, N. J. & Zarnecki, J. C. Ejecta fragmentation in impacts into gypsum and water ice. *Icarus* **214**, 739–747 (2011).
47. Kietzig, A.-M., Hatzikiriakos, S. G. & Englezos, P. Physics of ice friction. *J. Appl. Phys.* **107**, 081101 (2010).
48. Kennedy, F. E., Schulson, E. M. & Jones, D. E. The friction of ice on ice at low sliding velocities. *Philos. Mag. A* **80**, 1093–1110 (2000).
49. Crosta, G. B., Imposimato, S. & Roddeman, D. Numerical modeling of 2-D granular step collapse on erodible and nonerodible surface. *J. Geophys. Res.* **114**, F03020 (2009).
50. Hibert, C., Mangeney, A., Grandjean, G. & Shapiro, N. Slope instabilities in the Dolomieu crater, Réunion Island: from seismic signals to rockfall characteristics. *J. Geophys. Res.* **116**, F04032 (2011).
51. Roche, O., Montserrat, S., Niño, Y. & Tamburrino, A. Experimental observations of water-like behavior of initially fluidized, unsteady dense granular flows and their relevance for the propagation of pyroclastic flows. *J. Geophys. Res.* **113**, B12203 (2008).
52. Ancey, C., Coussot, P. & Evesque, P. A theoretical framework for granular suspension in a steady simple shear flow. *J. Rheol.* **43**, 1673–1699 (1999).
53. Savage, S. The mechanics of rapid granular flows. *Adv. Appl. Mech.* **24**, 289–366 (1984).
54. Di Toro, G. *et al.* Fault lubrication during earthquakes. *Nature* **471**, 494–498 (2011).
55. da Cruz, F., Emam, S., Prochnow, M., Roux, J. N. & Chevoir, F. Rheophysics of dense granular materials: discrete simulation of plane shear flows. *Phys. Rev. E* **72**, 021309 (2005).
56. Brodu, N., Richard, P. & Delannay, R. Shallow granular flows down flat frictional channels: steady flows and longitudinal vortices. *Phys. Rev. E* **87**, 022202 (2013).
57. Torson, J. & Becker, K. ISIS—a software architecture for processing planetary images. *LPSC XXVIII*, 1443–1444 (1997).
58. Moratto, Z. M., Broxton, M. J., Beyer, R. A., Lundy, M. & Husmann, K. Ames Stereo Pipeline, NASA's open source automated stereogrammetry software. *Lunar and Planetary Science Conference*. **41**, Abstract 2364 (2010).
59. Lucas, A. *Dynamique des Glissements de Terrain Par Modélisation Numérique et Télédétection: Application aux Exemples Martiens* (Thèse de doctorat, IPGP, 2010).
60. Pirulli, M. & Mangeney, A. Result of back-analysis of the propagation of rock avalanches as a function of the assumed rheology. *Rock Mech. Rock Eng.* **41**, 59–84 (2008).
61. Mangeney, A., Staron, L., Volfson, D. & Tsimring, L. Comparison between discrete and continuum modeling of granular spreading. *WSEAS Trans. Math.* **2**, 373–380 (2006).
62. King, J. P. Natural terrain landslide study—The natural terrain landslide inventory. *GEO Report No. 74. Hong Kong SAR: Geotechnical Engineering Office* (1999).
63. Quantin, C., Allemand, P. & Delacourt, C. Morphology and geometry of Valles Marineris landslides. *Planet. Space Sci.* **52**, 1011–1022 (2004).
64. Moore, M. *et al.* Mass movement and landform degradation on the icy Galilean satellites: results of the Galileo nominal mission. *Icarus* **140**, 294–312 (1999).
65. Schenk, P. & Bulmer, M. H. Thrust faulting, block rotation and large-scale mass movements at Euboea Montes, Io. *Science* **279**, 1514–1517 (1998).
66. Malin, C. M. Mass movements on Venus: preliminary results from Magellan cycle 1 observations. *J. Geophys. Res.* **97**, 16337–16352 (1992).

## Acknowledgements

The authors would like to thank J. Rice, N. Cubas, N. Lapusta, F. Passelègue, A. Schubnel, N. Brantut, M. Lapotre, J. Melosh, L. Moretti, A. Valance, P. Richard, R. Delannay, N. Brodu, O. Pouliquen, K. Miljković and O. Aharonson for interesting discussions and feedback. The authors also thank the French Space Agency (CNES) for its support. The research was funded by French ANR PLANETEROS and LANDQUAKES, by the Terrestrial Hazard Observation and Reporting (THOR) Center at Caltech and by Campus Spatial Grant from Université Paris-Diderot.

## Author contributions

A.L. collected the data, ran the numerical simulations, derived the digital terrain models, produced the figures and supplementary information ancillary materials and played a major role in the quantitative analysis. A.M. supervised the numerical analysis. A.L. and A.M. carried out the analytical development. J.P.A. developed the perspective on friction weakening processes from earthquake science. All the authors shared ideas, contributed to the interpretation of the results and to writing the manuscript.

## Additional information

**Supplementary Information** accompanies this paper at <http://www.nature.com/naturecommunications>

**Competing financial interests:** The authors declare no competing financial interests.

**Reprints and permission** information is available online at <http://npg.nature.com/reprintsandpermissions/>

**How to cite this article:** Lucas, A. *et al.* Frictional velocity-weakening in landslides on Earth and on other planetary bodies. *Nat. Commun.* 5:3417 doi: 10.1038/ncomms4417 (2014).